Monthly Notices
of the
ROYAL ASTRONOMICAL SOCIETY

MNRAS **488,** 78–88 (2019)
Advance Access publication 2019 July 1

doi:10.1093/mnras/stz1675

J-PAS: forecasts on interacting dark energy from baryon acoustic oscillations and redshift-space distortions

A. A. Costa [1,2★] R. J. F. Marcondes,[1] R. G. Landim [1,3] E. Abdalla,[1] L. R. Abramo,[1] H. S. Xavier,[4] A. A. Orsi [5] N. Chandrachani Devi [6] A. J. Cenarro,[7] D. Cristóbal-Hornillos,[7] R. A. Dupke,[8,9] A. Ederoclite,[4] A. Marín-Franch,[7] C. M. Oliveira,[4] H. Vázquez Ramió,[5] K. Taylor[10] and J. Varela[7]

[1]*Instituto de Física, Universidade de São Paulo, Rua do Matão 1371, São Paulo, SP 05508-090, Brazil*
[2]*Center for Gravitation and Cosmology, College of Physical Science and Technology, Yangzhou University, Yangzhou 225009, China*
[3]*SLAC National Accelerator Laboratory, 2575 Sand Hill Rd., Menlo Park, CA 94025, USA*
[4]*Instituto de Astronomia, Geofísica e Ciências Atmosféricas, Universidade de São Paulo, Rua do Matão 1226, São Paulo, SP 05508-090, Brazil*
[5]*Centro de Estudios de Física del Cosmos de Aragón, Plaza de San Juan 1, E-44001 Teruel, Spain*
[6]*Instituto de Astronomía, Universidad Nacional Autónoma de México, A. P. 70-264, 04510 México, D.F., México*
[7]*Centro de Estudios de Física del Cosmos de Aragón (CEFCA), Unidad Asociada al CSIC, Plaza de San Juan 1, E-44001 Teruel, Spain*
[8]*Observatorio Nacional-MCTIC, Rua Jose Cristino 77, Rio de Janeiro, Brazil*
[9]*Department of Astronomy, University of Michigan, 1085 S. University, Ann Arbor, MI 48109, USA*
[10]*Instruments4, 4121 Pembury Place, La Cañada-Flintridge, CA 91011, USA*

Accepted 2019 June 12. Received 2019 June 12; in original form 2019 April 2

ABSTRACT

We estimate the constraining power of Javalambre-Physics of the Accelerated Universe Astrophysical Survey (J-PAS) for parameters of an interacting dark energy (DE) cosmology. The survey is expected to map several millions of luminous red galaxies, emission line galaxies, and quasars in an area of thousands of square degrees in the northern sky with precise photometric redshift measurements. Forecasts for the DESI and Euclid surveys are also evaluated and compared to J-PAS. Using the Fisher matrix approach, we find that J-PAS can place constraints on the interaction parameter comparable to those from DESI, with an absolute uncertainty of about 0.02, when the interaction term is proportional to the dark matter energy density, and almost as good, of about 0.01, when the interaction is proportional to the DE density. For the equation of state of DE, the constraints from J-PAS are slightly better in the two cases (uncertainties 0.04–0.05 against 0.05–0.07 around the fiducial value -1). Both surveys stay behind Euclid but follow it closely, imposing comparable constraints in all specific cases considered.

Key words: methods: data analysis – surveys – cosmological parameters – cosmology: theory – dark energy – large-scale structure of Universe.

1 INTRODUCTION

The lack of knowledge regarding the nature of the dark sector, especially the cosmic acceleration (Riess et al. 1998; Perlmutter et al. 1999), has led to a continuous endeavour to understand the origin of such accelerated expansion and its dynamics. Several ongoing and upcoming spectroscopic, photometric and radio surveys have been proposed to address this problem, including DES (The Dark Energy Survey Collaboration 2005), LSST (LSST Science Collaboration 2009), eBOSS (Dawson et al. 2016), DESI (DESI Collaboration 2016), Euclid (Laureijs et al. 2011), BINGO (Battye et al. 2012; Wuensche & the BINGO Collaboration 2018), and SKA (Maartens et al. 2015). Among them, the Javalambre-Physics of the Accelerated Universe Astrophysical Survey (J-PAS, Benitez et al. 2009, 2014) is a multinarrow-band photometric survey that will cover up to 8500 deg^2 of the northern sky and measure $0.003(1+z)$ precision photometric redshifts for 9×10^7 luminous red galaxies (LRGs) and emission line galaxies (ELGs) plus several millions of quasars (QSO). In addition, it aims to detect and measure the mass of 7×10^5 galaxy clusters and groups, improving the constrains on dark energy (DE).

On the theoretical side, deviations from the Λ cold dark matter (ΛCDM) model have been proposed over the years, whose

★ E-mail: alencar@if.usp.br

alternatives to the cosmological constant include canonical and non-canonical scalar fields (Peebles & Ratra 1988; Ratra & Peebles 1988; Frieman, Hill & Watkins 1992; Frieman et al. 1995; Caldwell, Dave & Steinhardt 1998), holographic DE (Hsu 2004; Li 2004), vector fields (Armendariz-Picon 2004), metastable dark DE (Stojkovic, Starkman & Matsuo 2008), among others. One interesting possibility to consider is when we allow an exchange of energy–momentum between the two components of the dark sector (Wetterich 1995; Amendola 2000). This mechanism could be one reason why DE and dark matter (DM) contribute to the present Universe with comparable energy densities, alleviating the coincidence problem (Zimdahl, Pavón & Chimento 2001; Chimento et al. 2003). Models of interacting DE have been widely explored in the literature (Wang et al. 2016).

In this work, we consider a phenomenological description of the DE–DM interaction and use the Fisher matrix formalism to assess the capability of baryon acoustic oscillations (BAOs) and redshift-space distortions (RSDs), as observed by J-PAS, to improve the constraints on the equation of state (EoS) of DE and on the coupling constant. We also take advantage of the added power from combining multiple tracers of large-scale structure in order to improve the accuracy of measurements of the matter growth rate (Abramo & Leonard 2013; Abramo, Secco & Loureiro 2016; Marín et al. 2016; Witzemann et al. 2019). Our results are compared with those obtained for the Euclid and DESI surveys using the same methodology.

The paper is organized as follows. Section 2 introduces the interacting model, which we analyse in three specific cases. In Section 3, we describe the details of the surveys considered here. Section 4 explains how the RSD parameter changes in a interacting DE model. Our Fisher matrix analysis is presented in Section 5 and Section 6 contains our results, including a comparison with forecasts from the DESI and Euclid surveys. Section 7 is reserved for conclusions.

2 THE INTERACTING DARK ENERGY MODEL

The dark sector constitutes about 95 per cent of the energy density of the Universe. Its components, dubbed DM and DE, do not have a definitive model yet. Besides, their energy densities are of the same order of magnitude despite the fact they evolve completely different in the standard ΛCDM model. Hence, it seems natural to assume they can interact with each other. In this case, the energy–momentum tensors $T^{\mu\nu}_{(\lambda)}$ of each component λ are not independently conserved anymore,

$$\nabla_\mu T^{\mu\nu}_{(\lambda)} = Q^\nu_{(\lambda)}, \tag{1}$$

where $Q^\nu_{(\lambda)}$ is the four-vector that accounts for the coupling and satisfies the constraint $\sum_\lambda Q^\nu_{(\lambda)} = 0$.

Assuming a flat Friedmann–Lemaitre–Robertson–Walker (FLRW) universe, the conservation equations (1) give rise to the continuity equations (Marcondes et al. 2016; Costa et al. 2017)

$$\begin{aligned} &\dot\rho_c + 3H\rho_c = Q, \\ &\dot\rho_d + 3H\,(1+w)\,\rho_d = -Q, \end{aligned} \tag{2}$$

where $H = \dot a/a$ is the Hubble rate, Q is the coupling, and ρ_c and ρ_d are the background energy densities of DM and DE, respectively. The DE EoS is given by $w = P_d/\rho_d$, where P_d is its pressure. Throughout this work a dot represents derivative with respect to the cosmic time t.

From the continuity equations (2), we see that a positive Q indicates an energy transfer from DE to DM. General interactions including a field derived from Lagrangian models have been considered in other works (Micheletti, Abdalla & Wang 2009; Costa, Olivari & Abdalla 2015; D'Amico, Hamill & Kaloper 2016; Landim & Abdalla 2017). However, as we still do not know the correct theory to describe DM and DE, we can investigate an interaction between them from phenomenological arguments. In this work, we assume a phenomenological coupling Q that, in the generic case, have contributions proportional to the DM and DE densities

$$Q = 3H\,(\xi_c\rho_c + \xi_d\rho_d)\,, \tag{3}$$

where ξ_c and ξ_d are the corresponding coupling constants.

Table 1. Stability conditions on the EoS and interaction sign for the phenomenological interacting DE model.

Case	Constant EoS and interaction sign
$Q \propto \rho_d$ $(\xi_c = 0)$	$w < -1$ and $\xi_d > 0$; or
	$-1 < w < 0$ and $\xi_d < 0$
$Q \propto \rho_c$ $(\xi_d = 0)$	$w < -1$, $\forall\,\xi_c$
$\xi_d \neq 0$ and $\xi_c \neq 0$	$w < -1$, $\xi_d > 0$, $\forall\,\xi_c$

Interacting DE models with constant EoS have already been shown to suffer from instabilities with respect to curvature and DE perturbations (Väliviita, Majerotto & Maartens 2008; He, Wang & Abdalla 2009). Table 1 summarizes the allowed regions for the interaction and the DE EoS parameters as shown by He et al. (2009) and Gavela et al. (2009). However, this is likely a problem related to the oversimplicity of the interaction, which can be overcome in a more sophisticated Lagrangian description as in Costa et al. (2015). In fact, Yang et al. (2018) yield a phenomenological model with an interaction dependent on the DE EOS, which is stable in the whole parameter space with an interaction parameter greater than zero. See also Wang et al. (2016) for a review on interacting models.

3 THE DATA SET

The data considered correspond to the two-point function or, more precisely, the power spectrum of the clustering of some type of galaxy or quasar. J-PAS will be able to detect millions of LRGs, ELGs, and quasars. Table 2 gives the expected number densities as a function of redshift for different tracers. In the plane-parallel (distant observer, $k^2 = k_\parallel^2 + k_\perp^2$) approximation, the observed galaxy power spectrum is given by (Seo & Eisenstein 2003; Wang et al. 2010)

$$P_{g,\,\rm obs} = \left[\frac{D_A^{\rm fid}(z)}{D_A(z)}\right]^2 \frac{H(z)}{H^{\rm fid}(z)} \left[\sigma_{8,\,g}(z) + b\,\beta(z)\,\sigma_{8,\,m}\,\mu^2\right]^2 C(k) + P_{\rm shot}. \tag{4}$$

The prefactors, due to the Alcock–Paczynski effect (Alcock & Paczyński 1979), account for deviations from the fiducial Hubble rate and angular diameter distance to the true cosmology ones. $\sigma_{8,\,g} = b\,\sigma_{8,\,m}$, where $\sigma_{8,\,m}$ is the variance of the matter density field averaged in spheres of radius 8 h^{-1} Mpc and b is a bias between matter and galaxy overdensities. The RSD parameter β is equal to the matter growth rate divided by the bias, f_m/b. $\mu = k_\parallel/k$ is the cosine of the angle between the wavevector and the line of sight, $C(k) \equiv P_m(k,z)/\sigma^2_{8,\,m}(z) = P_{0,\,m}(k)/\sigma^2_{8,\,0}$ is the normalized true matter power spectrum and $P_{\rm shot}$ parametrizes a residual shot noise.

The galaxy overdensity is related to the matter overdensity through a bias, $\delta_g = b(k,z)\,\delta_m$, which in general can be a function of the scale and redshift. Here, we assume that the bias depends

Table 2. Number densities of LRGs, ELGs, and quasars for J-PAS, in units of $10^{-5}\,h^3\,\mathrm{Mpc}^{-3}$. The factor 10^{-5} in the unit here and in the following tables is to allow a better comparison.

z	LRG	ELG	QSO
0.3	226.6	2958.6	0.45
0.5	156.3	1181.1	1.14
0.7	68.8	502.1	1.61
0.9	12.0	138.0	2.27
1.1	0.9	41.2	2.86
1.3	0	6.7	3.60
1.5	0	0	3.60
1.7	0	0	3.21
1.9	0	0	2.86
2.1	0	0	2.55
2.3	0	0	2.27
2.5	0	0	2.03
2.7	0	0	1.81
2.9	0	0	1.61
3.1	0	0	1.43
3.3	0	0	1.28
3.5	0	0	1.14
3.7	0	0	0.91
3.9	0	0	0.72

Table 3. Number densities of LRGs, ELGs, and quasars for DESI, in units of $10^{-5}\,h^3\,\mathrm{Mpc}^{-3}$.

z	LRG	ELG	QSO
0.65	49	18	2.8
0.75	49	110	2.7
0.85	29	83	2.6
0.95	10	81	2.6
1.05	2.0	51	2.6
1.15	1.0	45	2.5
1.25	0	42	2.5
1.35	0	15	2.5
1.45	0	13	2.4
1.55	0	9.0	2.4
1.65	0	3.0	2.3
1.75	0	0	2.3
1.85	0	0	2.2

only on the redshift and is given, for each tracer, by (Ross et al. 2009; DESI Collaboration 2016)

$$b_{\mathrm{LRG}}(z) = \frac{1.7}{D(z)}, \quad b_{\mathrm{ELG}}(z) = \frac{0.84}{D(z)},$$
$$b_{\mathrm{QSO}}(z) = 0.53 + 0.289\,(1+z)^2\,, \tag{5}$$

where $D(z) = \exp\left[-\int_0^z \mathrm{d}z'\, f_m/\left(1+z'\right)\right]$ is the growth factor normalized to 1 today and $f_m = \mathrm{dln}\,\delta_m/\mathrm{dln}\,a$ is the matter growth rate. In our calculations we use weak Gaussian priors for the biases, with variances $\sigma_b = 0.5$.

We also compare our results for J-PAS with the expected results from DESI and Euclid. The number densities we are assuming are presented in Table 3 for the DESI survey and in Table 4 for Euclid. DESI has the same bias as those in equation (5); on the other hand, we use $b(z) = \sqrt{1+z}$ in the case of Euclid (Orsi et al. 2010; Wang et al. 2010; Laureijs et al. 2011). This choice of bias is a good approximation to studies from semi-analytic models of galaxy formation as in Orsi et al. (2010) (see e.g. Giannantonio et al. 2012). Although this choice is different from the one made for J-PAS and DESI, our results are only weakly dependent on it as we are considering information from the BAO wiggles only (Rassat et al. 2008).

Table 4. Number densities of ELGs for Euclid, in units of $10^{-5}\,h^3\,\mathrm{Mpc}^{-3}$.

z	ELG
0.6	356
0.8	242
1.0	181
1.2	144
1.4	99
1.8	33

Two scenarios are considered for the J-PAS survey, a more conservative initial expectation with a survey area of 4000 deg^2 and a possible future best case scenario with 8500 deg^2. The DESI and Euclid survey areas are estimated as 14 000 and 15 000 deg^2, respectively. The redshift errors are assumed to be $0.003(1+z)$ for J-PAS and $0.001(1+z)$ for DESI and Euclid.

4 THE MODIFIED RSD PARAMETER

Measurements of β from the power spectra or peculiar velocities are based on its correspondence with the velocity divergence θ as established by the continuity equation. Since this equation is violated in interacting models, we must make sure to use the correct quantity that corresponds to the velocity field when confronting our model with observations or making forecasts for some experiment (see e.g. Marcondes et al. 2016; Borges & Wands 2017; Kimura et al. 2018).

For an interacting DE model with coupling given by equation (3), the continuity equation for DM at first order in perturbations in the sub-horizon limit ($k \gg H$) reads

$$\delta_c' + 3\mathcal{H}\xi_d\frac{\rho_d}{\rho_c}\left(\delta_c - \delta_d\right) + \theta_c = 0. \tag{6}$$

In this equation, we now express, for convenience, the evolution in terms of the conformal time τ, with the prime representing $\mathrm{d}/\mathrm{d}\tau$ and $\mathcal{H} = a'/a$. The total matter density is $\rho_m = \rho_b + \rho_c$ and its perturbation $\delta_m = (\rho_b\delta_b + \rho_c\delta_c)/\rho_m$. Thus, its (conformal) time derivative is given by

$$\rho_m\delta_m' = -3\mathcal{H}\xi_c\rho_c\left(\delta_m - \delta_c\right) - 3\mathcal{H}\xi_d\rho_d\left(\delta_m - \delta_d\right) - \left(\rho_b\theta_b + \rho_c\theta_c\right), \tag{7}$$

where the continuity equations for baryons and DM have been used. This expression can be rewritten as

$$\mathcal{H}\left[\frac{\mathrm{d}\ln\delta_m}{\mathrm{d}\ln a} + 3\xi_c\frac{\rho_c}{\rho_m}\left(1 - \frac{\delta_c}{\delta_m}\right) + 3\xi_d\frac{\rho_d}{\rho_m}\left(1 - \frac{\delta_d}{\delta_m}\right)\right]\delta_m + \frac{\rho_b\theta_b + \rho_c\theta_c}{\rho_m} = 0. \tag{8}$$

We can now recognize the term $(\rho_b\theta_b + \rho_c\theta_c)/\rho_m$ as θ_m, as usual, and express the continuity equation corrected for the interaction

$$\mathcal{H}\tilde{f}_m\delta_m + \theta_m = 0, \tag{9}$$

where

$$\tilde{f}_m \equiv \frac{\mathrm{d}\ln\delta_m}{\mathrm{d}\ln a} + 3\left(\frac{\xi_c\rho_c + \xi_d\rho_d}{\rho_m} - \frac{\xi_c\rho_c\delta_c + \xi_d\rho_d\delta_d}{\rho_m\delta_m}\right) \tag{10}$$

is the growth rate for the interacting model minus the effects of interaction (to make the continuity equation compatible with RSD

measurements). This represents contributions from two averages of the two coupling constants ξ_c and ξ_d; one is weighted by the background densities of DE and DM, the other, with opposite sign, weighted by the perturbation to the densities.

Keeping the assumption that galaxies trace the matter field according to $\delta_g = b\,\delta_m$ and $\theta_g = \theta_m = \theta$, the galaxy continuity equation is now

$$\mathcal{H}\,\tilde{\beta}\,\delta_g + \theta = 0, \tag{11}$$

where $\tilde{\beta} \equiv \tilde{f}_m/b$ is the quantity that must replace β in equation (4) for the interacting model.

5 THE FISHER MATRIX FORMALISM

The Fisher matrix for the parameters ϑ_i of a model $\mathcal{M}$ is defined as the ensemble average of the Hessian matrix of the log likelihood. Assuming Gaussian fields with zero mean and covariance $\mathbf{C}$, the Fisher matrix is given by

$$F_{ij} \equiv \left\langle -\frac{\partial \ln \mathcal{L}}{\partial\vartheta_i\,\partial\vartheta_j} \right\rangle = \frac{1}{2}\mathrm{Tr}\left[\mathbf{C}^{-1}\frac{\partial\mathbf{C}}{\partial\vartheta_i}\mathbf{C}^{-1}\frac{\partial\mathbf{C}}{\partial\vartheta_j}\right]. \tag{12}$$

For the case of a galaxy power spectrum, the Fisher matrix components for a single tracer results in

$$F_{g,\,ij} = \frac{1}{2}\int \frac{\mathrm{d}^3k}{(2\pi)^3}\,V_{g,\,\mathrm{eff}}\,\frac{\partial \ln P_{g,\,\mathrm{obs}}}{\partial\vartheta_i}\frac{\partial \ln P_{g,\,\mathrm{obs}}}{\partial\vartheta_j}. \tag{13}$$

The effective volume is defined as (Feldman, Kaiser & Peacock 1994; Tegmark 1997)

$$V_{g,\,\mathrm{eff}}(k) = \int_V \mathrm{d}^3x\,\left[\frac{n_g(z)P_g(k,z)}{1+n_g(z)P_g(k,z)}\right]^2, \tag{14}$$

where $n_g(z)$ is the number density of galaxies and $P_g(k, z)$ is the galaxy power spectrum given by equation (4). However, in practice the information that can be extracted from photometric surveys is limited both by the photometric redshift accuracy and the mode-mixing that takes place due to non-linear structure formation, and for these reasons we redefine the effective volume as

$$V_{g,\,\mathrm{eff}} \to \int_V \mathrm{d}^3x\,\left[\frac{n_g(z)P_g(k,z)}{1+n_g(z)P_g(k,z)}\right]^2 \mathrm{e}^{-2\mu^2\delta_z^2k^2\left(\frac{1+z}{H(z)}\right)^2} \times \mathrm{e}^{-k^2\Sigma_\perp^2 - k^2\hat{\mu}^2\left(\Sigma_\parallel^2-\Sigma_\perp^2\right)}. \tag{15}$$

The first exponential factor in equation (15) comes from assuming Gaussian errors for the photometric redshifts, with variance $\sigma_z = \delta_z(1+z)$. The second exponential factor yields a cut-off to avoid non-linear scales (Takada et al. 2014), where $\Sigma_\parallel = c_{\mathrm{rec}}D(z)\,\Sigma_0$ and $\Sigma_\perp = c_{\mathrm{rec}}D(z)(1+f)\Sigma_0$. The constant c_{rec} is introduced to model the reconstruction method of the BAO peaks. Without reconstruction, $c_{\mathrm{rec}} = 1$, which is the value we assume in this paper. $D(z)$ is the growth function normalized as $D(z=0) = 1$ and we use $\Sigma_0 = 11\,h^{-1}$ Mpc.

The Fisher matrix given by equations (13) and (15) allows us to define the Fisher information density per unit of phase space volume $(2\pi)^{-3}\,\mathrm{d}^3x\,\mathrm{d}^3k$ as (aside from the phenomenological exponential factors)

$$\Phi = \frac{1}{2}\left[\frac{n_g(z)P_g(k,z)}{1+n_g(z)P_g(k,z)}\right]^2. \tag{16}$$

For surveys that are able to combine multiple tracers of large-scale structure, the Fisher information density can be generalized to (Abramo & Leonard 2013)

$$\Phi_{\alpha\beta}(x,k) = \frac{1}{4}\left[\delta_{\alpha\beta}U_\alpha X + U_\alpha U_\beta\,(1-X)\right], \tag{17}$$

where $\alpha, \beta = 1, \ldots, N$ are the different types of galaxies, $X_\alpha = n_\alpha P_\alpha(k, z)$ such that $X = \sum_\alpha X_\alpha$, and $U_\alpha = X_\alpha/(1+X)$. Hence, the Fisher matrix can be generalized for a multitracer analysis as

$$F_{ij} = \sum_{\alpha,\,\beta=1}^{N}\int \frac{\mathrm{d}^3x\,\mathrm{d}^3k}{(2\pi)^3}\,\frac{\partial \ln X_\alpha}{\partial\vartheta_i}\Phi_{\alpha\beta}\frac{\partial \ln X_\beta}{\partial\vartheta_j}\mathrm{e}^{-\mu^2\delta_{z,\,\alpha}^2k^2\left(\frac{1+z}{H(z)}\right)^2} \times \mathrm{e}^{-\mu^2\delta_{z,\,\beta}^2k^2\left(\frac{1+z}{H(z)}\right)^2}\,\exp\left[-k^2\Sigma_\perp^2 - k^2\hat{\mu}^2(\Sigma_\parallel^2-\Sigma_\perp^2)\right]. \tag{18}$$

Using this expression we can properly take into account multiple tracers in our analysis. For instance, we can combine the expected results from LRG, ELG, and QSO, all together.

Another important result is that we can transform a Fisher matrix defined in terms of a set of N_ϑ parameters, $\{\vartheta^i\}$, into a set of N_φ parameters, $\{\varphi^\alpha\}$, as long as $N_\varphi \leq N_\vartheta$. The Fisher matrix transformation is defined by

$$F_{\alpha\beta} = \sum_{i,\,j}^{N_\vartheta}\frac{\partial\vartheta^i}{\partial\varphi^\alpha}F_{ij}\frac{\partial\vartheta^j}{\partial\varphi^\beta}. \tag{19}$$

In our analysis, we begin with a set of parameters $\vartheta^i = \{\ln H(z), \ln D_A(z), f_s(z), \sigma_{8,\,g}(z), P_{\mathrm{shot}}, \Omega_b h^2, \Omega_c h^2, h, n_s\}$, where $f_s(z) = \tilde{f}_m(z)\sigma_{8,\,m}(z)$. Note that some parameters are local, i.e. they assume different values at each redshift bin, while others are global. For a multispecies analysis, each tracer has its own bias and, hence, different values of $\sigma_{8,\,g}$. Later, we marginalize over all those parameters except $\ln H(z)$, $\ln D_A(z)$ and $f_s(z)$, which carry all the information about BAO and RSD. Finally, we project from those parameters to our final set of cosmological parameters, which are given here by Ω_d, w, ξ_c, and ξ_d.

Our fiducial cosmology is a flat ΛCDM model with a physical baryon density $\Omega_b h^2 = 0.0226$, CDM density $\Omega_c\,h^2 = 0.121$, and neutrino density parameter, $\Omega_\nu\,h^2 = 0.00064$ (assuming only one massive neutrino). The reduced Hubble constant is $h = 0.68$ (with a prior $\sigma_h = 0.1$), DE EOS $w = -1$, amplitude parameter $A_s = 2.1 \times 10^{-9}$ and scalar spectral index $n_s = 0.96$. Planck priors are used to calibrate the BAO scale only.

Our Fisher code receives as input background and perturbed quantities such as the Hubble rate and the linear matter power spectrum, which were calculated using a modified version of the CAMB code (Lewis, Challinor & Lasenby 2000; Costa 2014; Costa et al. 2014) that takes into account the necessary modifications for an interacting DE model.

6 RESULTS

We now present the expected constraints on the parameters, as well as the two-parameter joint constraints for the different cases of our interacting model. Two scenarios are considered: one using information from $H(z)$ and $D_A(z)$ only, and the other adding information from $f_s(z)$ besides $H(z)$ and $D_A(z)$. The two cases are labelled 'without RSD' and 'with RSD' and, in both, we run our analysis for the two J-PAS survey areas described in Section 3. We are also conservative regarding the number density of quasars, taking 90 per cent of the densities predicted in previous work (Abramo et al. 2012), and the ability to recover quasi-non-linear scales (reconstruction), which means that if we achieve successful

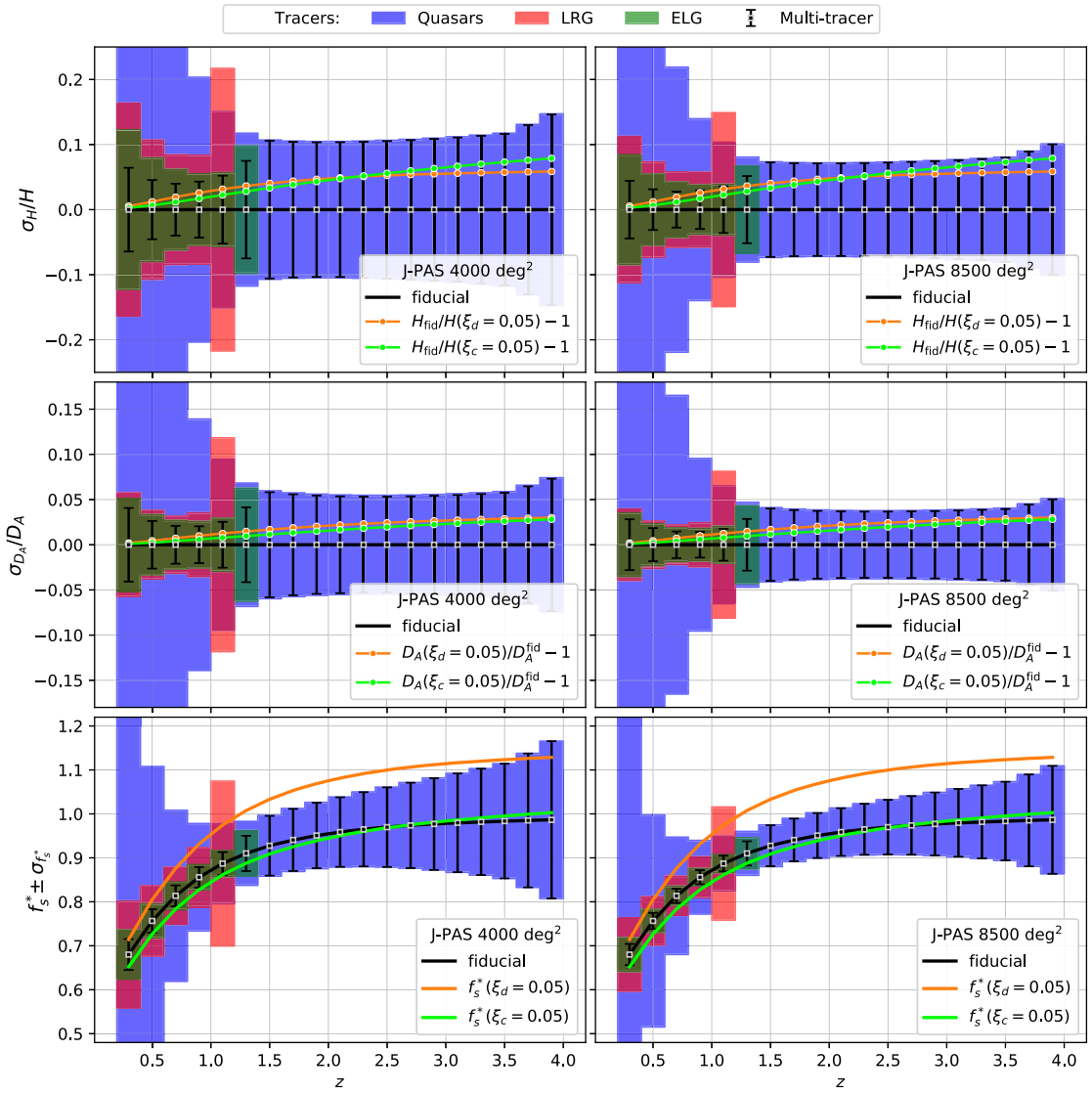

Figure 1. Predicted uncertainties on $H(z)$, $D_A(z)$, and $f_s^*(z) \equiv f_s(z)/\sigma_{8,m}^{\rm fid}(z)$ from LRG, ELG, QSO and the three tracers combined, considering the survey areas of 4000 and 8500 deg^2. We also show the effect, on those functions, of an interaction strength of magnitude 0.05 in the cases $Q \propto \rho_d$ and $Q \propto \rho_c$.

reconstruction with J-PAS, then the constraints from the actual data could be further improved.

Note that we are more concerned here with the marginalized uncertainties on the parameters, under the assumption that they should not vary considerably over the parameter space, i.e. they are not strongly dependent on the choice of fiducial parameters. In fact, one should note that these results do not include any prior information about the allowed region for Ω_d, w, and ξ_i, which will certainly not be true in the actual data analysis when we will have to restrict the parameters to the stability regions listed in Table 1.

The uncertainties on $H(z)$, $D_A(z)$, and $f_s(z)$ are shown in Fig. 1 together with the effect of the interaction on these functions. We can see that an interacting DE induces deviations from our fiducial cosmology. This effect is stronger for higher redshifts in $H(z)$, $D_A(z)$, and $f_s(z)$ with $Q \propto \rho_d$. Thus, quasars at high redshifts are expected to produce competitive constraints on the interaction in our models.

Before we discuss our results, we would like to emphasize that when the interaction is proportional to the DE density, we have two distinct regions of stability. One is characterized by the DE EOS in the phantom regime $w < -1$, in which case the interaction must be positive, and the other quintessence-like case $-1 < w < 0$, for which Q must be negative. In the Fisher matrix analysis we perform here, there is no need to make explicit those two regions separately. The results are consistent with one another and, hence, we will not make such distinction hereafter. The reader, however, must be aware of the stable regions according to Table 1. For all the results below we use conservative Gaussian priors on the uncertainties of Ω_d, w, and ξ, with variances $\sigma_{\Omega_d} = 1$, $\sigma_w = 3$ and $\sigma_\xi = 1$.

The marginalized constraints for the case $Q \propto \rho_d$ are shown in Tables 5 (without RSD) and 6 (with RSD). We present the results for two J-PAS areas, together with the expected results for DESI and Euclid. We observe that, when information from RSD is not considered, our three parameters of interest are very degenerate. The constraints are dominated by our priors on Ω_d, w and ξ_d. None of the tracers or any survey was able to break this degeneracy and produce significant constraints. However, the inclusion of RSD introduces new information that alleviates the degeneracy. In this case, the prior uncertainties are not important and we obtain constraints of

Table 5. Marginalized uncertainties for the three surveys, without RSD, for the case where the interacting coupling term is proportional to DE density, $Q \propto \rho_d$. The parameters we are concerned, Ω_d, w, and ξ_d are observed to be very degenerated. The results are dominated by our priors.

	Uncertainty	LRG	ELG	QSO	Multitracer
J-PAS	σ_{Ω_d}	0.552	0.547	0.546	0.546
(4000 deg^2)	σ_w	0.856	0.813	0.811	0.798
	σ_{ξ_d}	0.800	0.796	0.795	0.795
J-PAS	σ_{Ω_d}	0.549	0.547	0.546	0.546
(8500 deg^2)	σ_w	0.824	0.803	0.803	0.796
	σ_{ξ_d}	0.797	0.796	0.795	0.795
DESI	σ_{Ω_d}	0.547	0.546	0.546	0.546
	σ_w	0.809	0.797	0.813	0.796
	σ_{ξ_d}	0.796	0.795	0.795	0.795
Euclid	σ_{Ω_d}		0.546		
	σ_w		0.795		
	σ_{ξ_d}		0.795		

Table 6. Marginalized uncertainties for the three surveys, with RSD, for the case where the interacting coupling term is proportional to DE density, $Q \propto \rho_d$. The inclusion of RSD information breaks the strong degeneracy presented before.

	Uncertainty	LRG	ELG	QSO	Multitracer
J-PAS	σ_{Ω_d}	0.064	0.030	0.024	0.011
(4000 deg^2)	σ_w	0.251	0.114	0.157	0.058
	σ_{ξ_d}	0.080	0.025	0.030	0.016
J-PAS	σ_{Ω_d}	0.044	0.021	0.016	0.008
(8500 deg^2)	σ_w	0.173	0.078	0.108	0.040
	σ_{ξ_d}	0.055	0.017	0.021	0.011
DESI	σ_{Ω_d}	0.032	0.013	0.026	0.010
	σ_w	0.145	0.058	0.162	0.047
	σ_{ξ_d}	0.041	0.009	0.026	0.008
Euclid	σ_{Ω_d}		0.006		
	σ_w		0.028		
	σ_{ξ_d}		0.004		

a few per cent as observed in Table 6. This can be compared with a similar analysis made in Santos et al. (2017) for an Euclid-like survey. We can see that our constraints for the DE EOS and the interaction parameter are comparable to those found in their tables III and IV. Comparing the multitracer analysis for the three surveys (actually we are not using multitracer for Euclid, only ELG), we see that J-PAS can produce slightly better constraints than DESI for the DE density parameter and the EOS. This is associated with the expected values for QSO, which are denser and reach higher redshifts in J-PAS. The joint constraints for Ω_d, w, and ξ_d are shown in Fig. 2 for the two areas and for the different tracers with J-PAS.

The same is done for the case $Q \propto \rho_c$, presented in Tables 7 (without RSD) and 8 (with RSD) and in Fig. 3. In this case, the resulting parameters are not as degenerate as in the previous case. The constraints on $H(z)$ and $D_A(z)$ can provide significant information and our prior is not as dominant as before. For instance, in the multitracer analysis, the prior uncertainties only alter our results at ∼2 per cent for J-PAS 4000 deg^2 and at ∼1 per cent for J-PAS 8500 deg^2. Table 7 shows us that J-PAS can put better constraints than DESI and Euclid when we only consider BAO information in this model. Again, the constraints from LRG, ELG, and QSO indicate that QSO are playing the role in this leadership

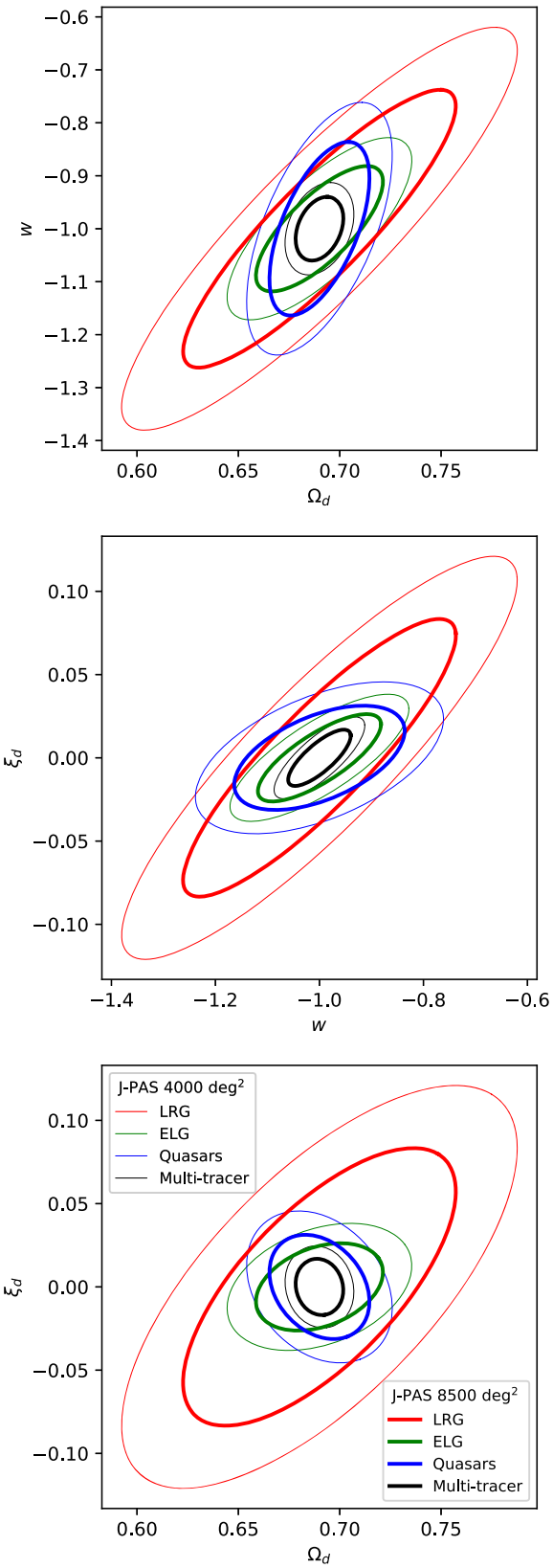

Figure 2. Case $Q \propto \rho_d$ ($\xi \equiv \xi_d$). The ellipses represent the 68 per cent uncertainty around the fiducial ΛCDM model. The thin and thick lines correspond to results considering the survey areas of 4000 and 8500 deg^2, respectively. The red contours are for LRG, green for ELG, blue for QSO, and black for the multitracer analysis, all with RSD.

Table 7. Marginalized uncertainties for the three surveys, without RSD, for the case where the interacting coupling term is proportional to DM density, $Q \propto \rho_c$. J-PAS (8500 deg^2) can put better constraints than DESI and Euclid in the multitracer analysis.

	Uncertainty	LRG	ELG	QSO	Multitracer
J-PAS (4000 deg^2)	σ_{Ω_d}	0.453	0.418	0.218	0.115
	σ_w	0.844	0.788	0.621	0.273
	σ_{ξ_c}	0.830	0.712	0.230	0.135
J-PAS (8500 deg^2)	σ_{Ω_d}	0.435	0.367	0.156	0.080
	σ_w	0.788	0.687	0.443	0.189
	σ_{ξ_c}	0.804	0.626	0.164	0.094
DESI	σ_{Ω_d}	0.419	0.215	0.361	0.144
	σ_w	0.775	0.436	0.807	0.292
	σ_{ξ_c}	0.746	0.333	0.500	0.220
Euclid	σ_{Ω_d}		0.096		
	σ_w		0.209		
	σ_{ξ_c}		0.134		

Table 8. Marginalized uncertainties for the three surveys, with RSD, for the case where the interacting coupling term is proportional to dark DM density, $Q \propto \rho_c$.

	Uncertainty	LRG	ELG	QSO	Multitracer
J-PAS (4000 deg^2)	σ_{Ω_d}	0.174	0.064	0.083	0.030
	σ_w	0.379	0.161	0.308	0.074
	σ_{ξ_c}	0.228	0.082	0.074	0.037
J-PAS (8500 deg^2)	σ_{Ω_d}	0.123	0.044	0.058	0.021
	σ_w	0.267	0.111	0.213	0.051
	σ_{ξ_c}	0.161	0.056	0.051	0.026
DESI	σ_{Ω_d}	0.122	0.030	0.076	0.025
	σ_w	0.284	0.086	0.243	0.071
	σ_{ξ_c}	0.146	0.030	0.076	0.026
Euclid	σ_{Ω_d}		0.012		
	σ_w		0.039		
	σ_{ξ_c}		0.013		

here. Including information from RSD can improve the results even more. However, the constraints in this case are not as sensitive to RSD as when $Q \propto \rho_d$, as could be expected from Fig. 1. J-PAS still provides better results than DESI with RSD information, but Euclid gives an uncertainty on the coupling constant twice as better. Also, in this case, we can compare our results with Santos et al. (2017). This time, our constraints in Table 8 are weaker than those found by them in their table V. In fact, their constraint for the interaction parameter is three times stronger than ours. However, this must be related with some differences between our analysis, as some dependence with the fiducial values. In any case, we have obtained a more conservative result.

For the last case considered, $Q \propto \rho_d + \rho_c$, we give the results for the marginalized constraints in Tables 9 (without RSD) and 10 (with RSD). As one could expect, in this scenario we see characteristics combined from both previous cases. The measurements of $H(z)$ and $D_A(z)$ give significant information, especially at high redshifts, as in $Q \propto \rho_c$. The constraints are also very sensitive to RSD as in $Q \propto \rho_d$.

Using information from BAO and RSD, we compare the expected confidence regions of J-PAS (8500 deg^2), DESI and Euclid, all with multiple tracers except Euclid, which has only one kind of tracer. The results for the cases $Q \propto \rho_d$ and $Q \propto \rho_c$ are presented in Figs 4

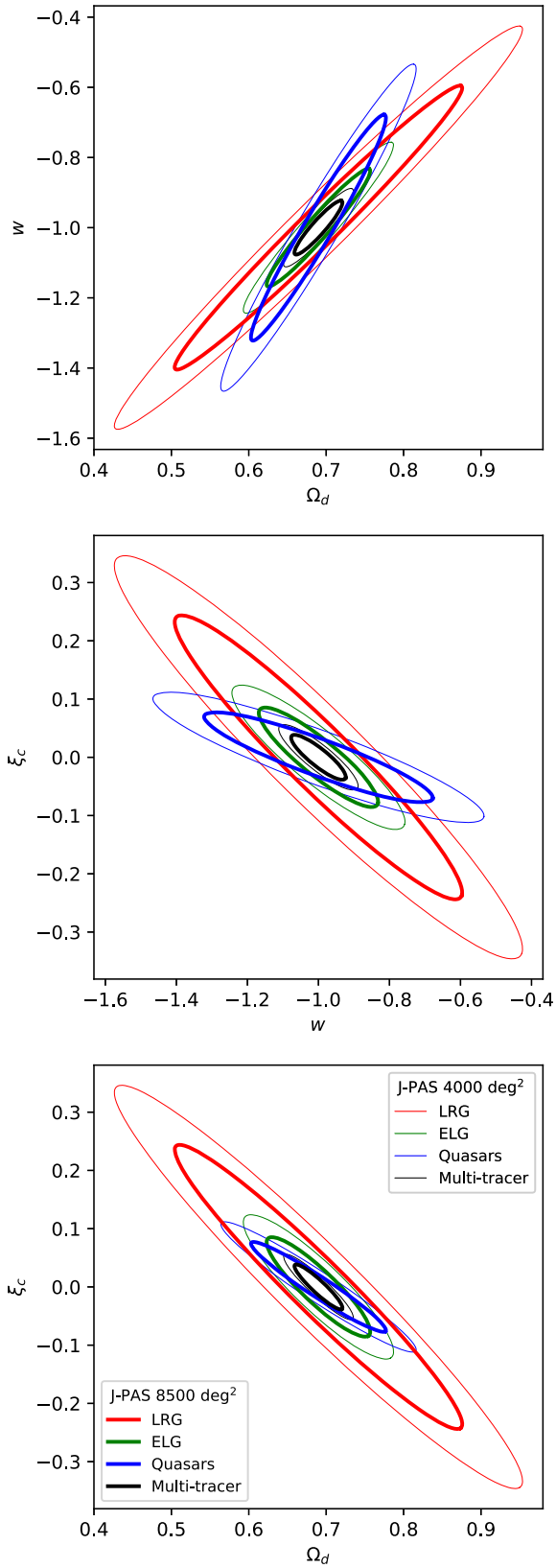

Figure 3. Case $Q \propto \rho_c$ ($\xi \equiv \xi_c$). The ellipses represent the 68 per cent uncertainty around the fiducial ΛCDM model. The thin and thick lines correspond to results considering the survey areas 4000 and 8500 deg^2, respectively. The red contours are for LRG, green for ELG, blue for QSO, and black for the multitracer analysis, all with RSD.

Table 9. Marginalized uncertainties for the three surveys, without RSD, for the case where the interacting coupling term is proportional to the sum of the dark sector energy densities, $Q \propto \rho_c + \rho_d$ ($\xi_c = \xi_d \equiv \xi$).

	Uncertainty	LRG	ELG	QSO	Multitracer
J-PAS	σ_{Ω_d}	0.708	0.670	0.354	0.204
(4000 deg^2)	σ_w	1.146	1.103	0.795	0.396
	σ_ξ	0.585	0.528	0.217	0.133
J-PAS	σ_{Ω_d}	0.697	0.623	0.260	0.143
(8500 deg^2)					
	σ_w	1.117	1.022	0.583	0.277
	σ_ξ	0.573	0.490	0.159	0.093
DESI	σ_{Ω_d}	0.679	0.406	0.578	0.284
	σ_w	1.104	0.701	1.069	0.490
	σ_ξ	0.546	0.305	0.412	0.212
Euclid	σ_{Ω_d}		0.185		
	σ_w		0.336		
	σ_ξ		0.132		

Table 10. Marginalized uncertainties for the three surveys, with RSD, for the case where the interacting coupling term is proportional to the sum of the dark sector energy densities, $Q \propto \rho_c + \rho_d$ ($\xi_c = \xi_d \equiv \xi$).

	Uncertainty	LRG	ELG	QSO	Multitracer
J-PAS	σ_{Ω_d}	0.051	0.030	0.058	0.019
(4000 deg^2)	σ_w	0.178	0.094	0.141	0.041
	σ_ξ	0.110	0.035	0.041	0.019
J-PAS	σ_{Ω_d}	0.035	0.021	0.040	0.013
(8500 deg^2)					
	σ_w	0.123	0.065	0.097	0.028
	σ_ξ	0.076	0.024	0.028	0.013
DESI	σ_{Ω_d}	0.024	0.012	0.034	0.011
	σ_w	0.093	0.048	0.127	0.038
	σ_ξ	0.054	0.013	0.036	0.011
Euclid	σ_{Ω_d}		0.008		
	σ_w		0.025		
	σ_ξ		0.006		

and 5. Even though Euclid has only one kind of tracer, it shows the best constraints in those figures. This is related to its large survey area, high galaxy number densities, and small redshift errors. On the other hand, although DESI covers a larger area in the sky and has a smaller redshift error than J-PAS, their constraints are comparable because of the larger redshift range of J-PAS.

It is important to notice that, in our analysis, we are not considering the Bright Galaxy Survey sample at low redshift from DESI Collaboration (2016).[1] As a simple flux-limited sample of galaxies, it will consist of different types of galaxies. Thus, one of the reasons to avoid this sample in our analysis is how to properly take it into account in our multitracer analysis. On the other hand, the basic strategy for galaxy clustering with Euclid does not possess low-redshift measurements (Laureijs et al. 2011), although, it is possible to add low-redshift data from other survey, such as the Sloan Digital Sky Survey (Blanton et al. 2017). Therefore, including those low-redshift data for DESI and Euclid would improve the constraints found for them in this paper.

[1]We thank Prof. Daniel Eisenstein to call our attention for that fact in a private communication.

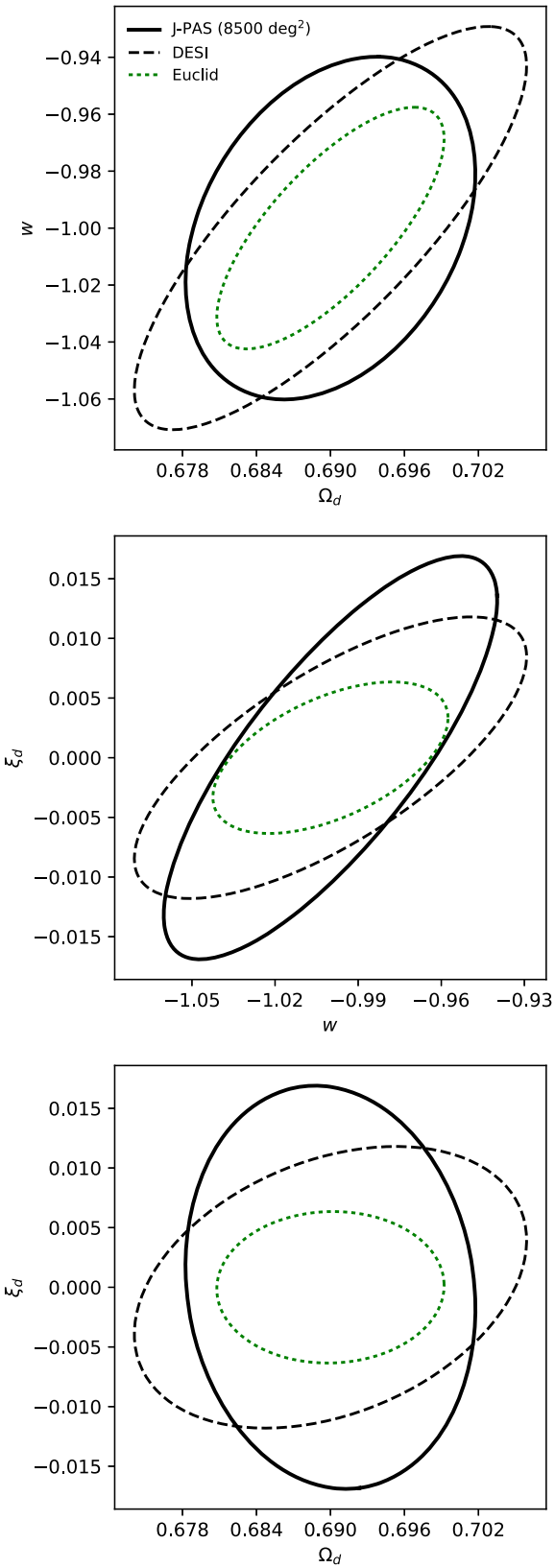

Figure 4. Comparison of the 68 per cent uncertainties around the fiducial ΛCDM model for the J-PAS (8500 deg^2), Euclid, and DESI surveys including information from BAO and RSD in a multitracer analysis. Case $Q \propto \rho_d$ ($\xi \equiv \xi_d$).

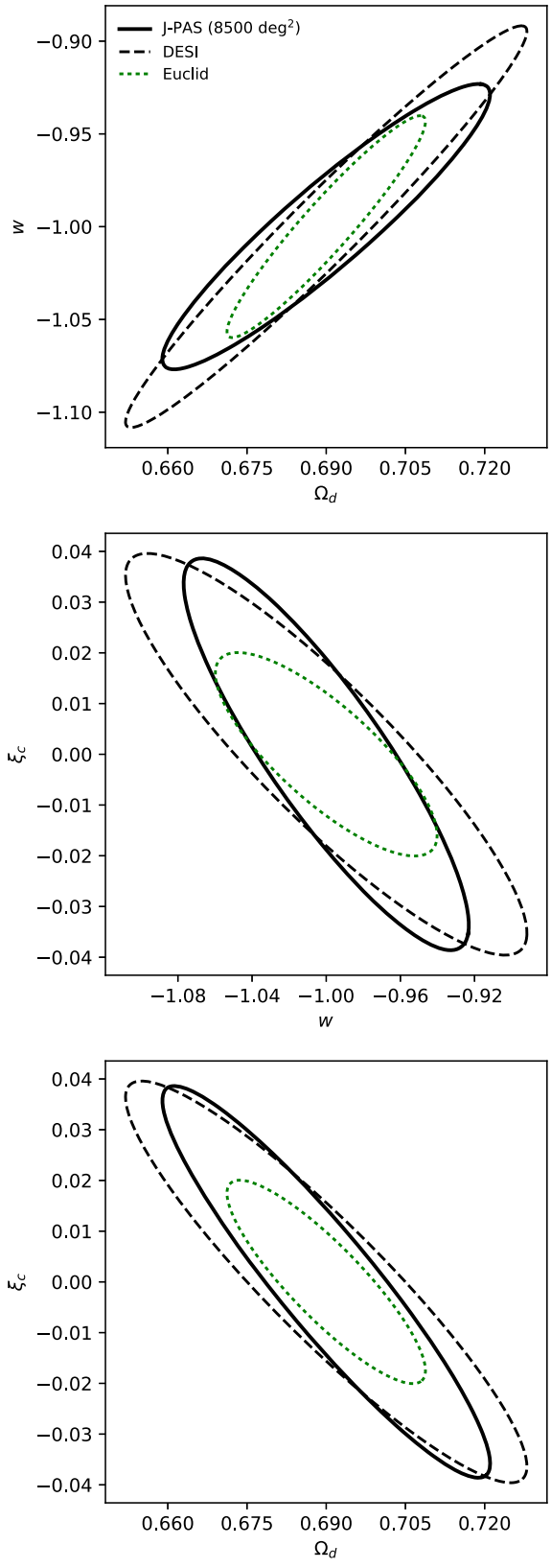

Figure 5. Comparison of the 68 per cent uncertainties around the fiducial ΛCDM model for the J-PAS (8500 deg^2), Euclid, and DESI surveys including information from BAO and RSD in a multitracer analysis. Case $Q \propto \rho_c$ ($\xi \equiv \xi_c$).

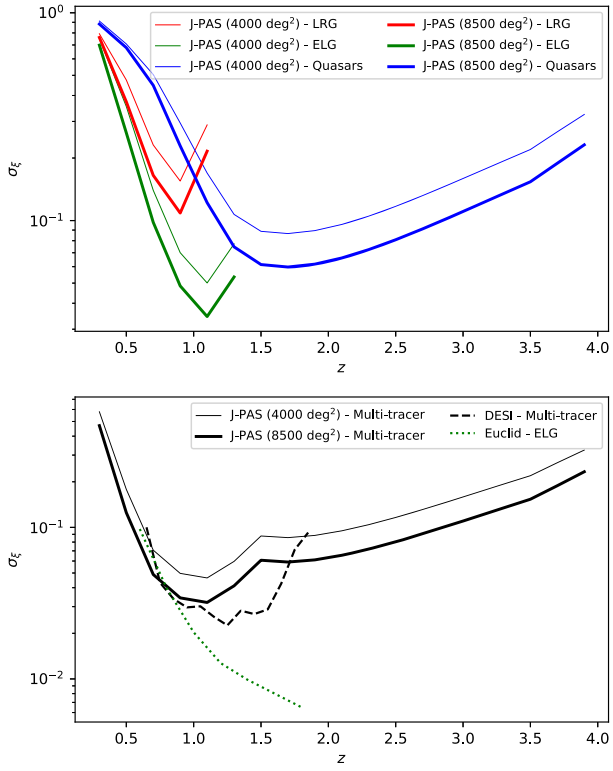

Figure 6. Constraint on ξ_d as a function of the redshift z under the different survey configurations, case $Q \propto \rho_d$ ($\xi \equiv \xi_d$).

Finally, we see that the results for our interacting DE model are very sensitive to the use of RSDs. This is certainly true for an interaction proportional to the DE density, where loose constraints dominated by our priors tighten considerably when we include RSD, but also in the other cases, in which the constraints can improve by a factor of 10 in some scenarios. This was also clear in previous publications (Murgia, Gariazzo & Fornengo 2016; Costa et al. 2017; Li et al. 2018). We note that high-redshift measurements tend to place better constraints, as the interaction yields stronger deviations from the standard model at those redshifts. Figs 6–8 summarize the interaction constraints as a function of the redshift, for the cases $Q \propto \rho_d$, $Q \propto \rho_c$, and $Q \propto \rho_c + \rho_d$, respectively. However, combining different tracers at various redshifts in a multitracer analysis have produced the best scenario. On the other hand, increasing the J-PAS survey area from 4000 to 8500 deg^2 induces a relative difference on the constraints of about 40 per cent.

7 CONCLUSIONS

In this work, we use information from BAO and RSDs to estimate the constraining power of the J-PAS survey for parameters of an interacting DE model. The analysis is done using the Fisher matrix formalism and Planck priors were only used to calibrate the BAO scale.

Employing the whole galaxy power spectrum, we marginalize over several cosmological parameters ending up with three local parameters, $\ln H(z)$, $\ln D_A(z)$, and $f_s(z)$, which basically carry information about the BAO scale and RSD. Then, we project the expected constraints on those parameters on constraints over our interacting DE model, which is described by the DE density fraction Ω_d, the EOS w, and the interaction parameter ξ_c or ξ_d.

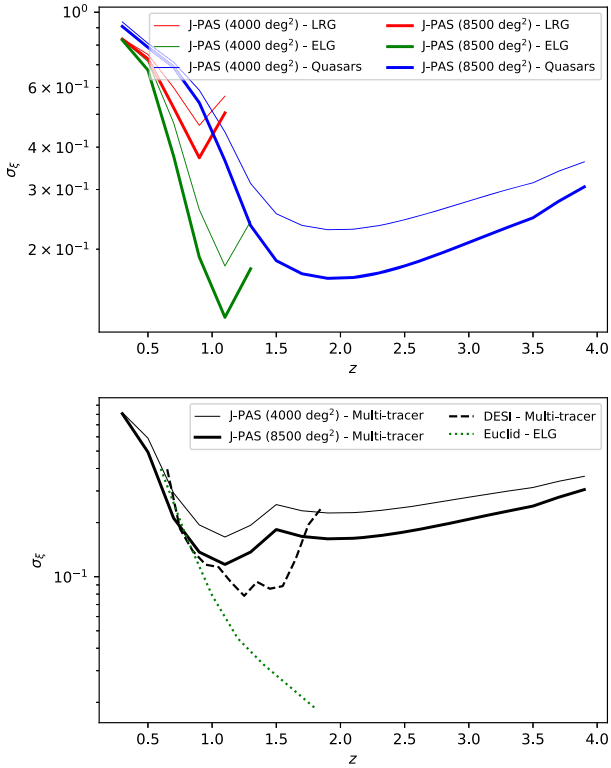

Figure 7. Constraint on ξ_c as a function of the redshift z under the different survey configurations, case $Q \propto \rho_c$ ($\xi \equiv \xi_c$).

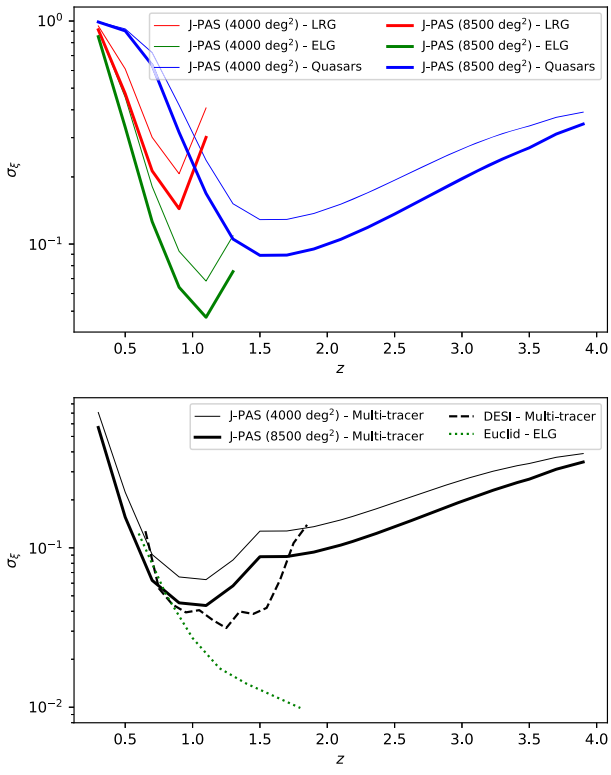

Figure 8. Constraint on ξ as a function of the redshift z under the different survey configurations, case $Q \propto \rho_c + \rho_d$ ($\xi_c = \xi_d \equiv \xi$).

We consider the effect of different tracers (i.e. LRG, ELG, and QSO) of the underlying matter distribution on the constraints and, also, a multitracer analysis. The impact of the survey area is also taken into account and the results are compared with those from DESI and Euclid.

We find that, with J-PAS data in the near future, we shall be able to determine the interaction parameter with a maximum precision of $\sigma_{\xi_c} \sim 0.02$ when the interaction term is proportional to the DM energy density and of $\sigma_{\xi_d} \sim 0.01$ when the interaction is proportional to the DE density. These numbers are similar to the constraints predicted by DESI. For the constant EOS of DE, the best predicted constraints from J-PAS are slightly better than those from DESI in both interacting cases: σ_w about 0.04–0.05 against 0.05–0.07 around the fiducial value $w = -1$. In terms of constraining power and in the context of our interacting model, both surveys are behind Euclid but get close to it, projecting comparable constraints on the relevant parameters in all specific cases considered.

Finally, we would like to emphasize some limitations and possible extensions of this work:

(i) As it is well known, the Fisher matrix formalism provides the best case scenario for a forecast. A natural extension should properly explore the space of parameters as in a Monte Carlo approach. In this case, the unstable regions presented in Table 1 would be avoided by some priors.

(ii) Also two aspects that could impair the J-PAS constraints in comparison to DESI and Euclid are a more realistic photo-z error distribution (with longer tails and more outliers than a Gaussian distribution) and the contamination of our galaxy sample by stars (and by tracers of a different type). This will become clearer in the next months with ongoing J-PAS proof-of-concept tests.

(iii) We have only taken into account contributions from BAO and RSD. However, J-PAS is able to do more. A more complete analysis could combine information from supernovae Type Ia, weak lensing and galaxy clusters.

(iv) At $z \geq 2$, J-PAS will be able to detect a significant population of Lyman α emitters (more numerous than QSOs) that is not taken into account in this analysis. This could significantly enhance the importance of high-z constraints.

(v) The likelihood function for every survey will depend strongly on the range of scales that is used to measure $P(k)$. This is especially important for RSD analysis. Also, the assembly bias, the description of non-linear density and velocity field regimes, and the impact of galaxy formation in general could make the modelling of RSDs significantly more challenging, e.g. Orsi & Angulo (2018). This could either bias the constraints, or dramatically weaken the contribution of RSDs to the overall constraints.

ACKNOWLEDGEMENTS

AAC acknowledges Fundação de Amparo à Pesquisa do Estado de São Paulo (FAPESP) and Coordenação de Aperfeiçoamento de Pessoal de Nível Superior (CAPES) for the financial support under grant number 2013/26496-2 (FAPESP). RGL is supported by Conselho Nacional de Desenvolvimento Científico e Tecnológico (CNPq) under the grant 208206/2017-5. EA acknowledges FAPESP (grant number 2014/07885-0) and CNPq for support. LRA thanks FAPESP and CNPq for financial support. RAD acknowledges support from CNPq through BP grant 312307/2015-2, and the Financiadora de Estudos e Projetos – FINEP grants REF 1217/13 – 01.13.0279.00 and REF 0859/10 - 01.10.0663.00 and also Fundação Carlos Chagas Filho de Amparo à Pesquisa do

Estado do Rio de Janeiro (FAPERJ), FAPERJ PRONEX grant E-26/110.566/2010 for hardware funding support for the J-PAS project through the National Observatory of Brazil and Centro Brasileiro de Pesquisas Físicas.

This paper has gone through internal review by the J-PAS collaboration. Funding for the J-PAS Project has been provided by the Governments of España and Aragón through the Fondo de Inversión de Teruel, European FEDER funding and the MINECO and by the Brazilian agencies FINEP, FAPESP, FAPERJ, and by the National Observatory of Brazil.

REFERENCES

Abramo L. R., Leonard K. E., 2013, MNRAS, 432, 318
Abramo L. R. et al., 2012, MNRAS, 423, 3251
Abramo L. R., Secco L. F., Loureiro A., 2016, MNRAS, 455, 3871
Alcock C., Paczyński B., 1979, Nature, 281, 358
Amendola L., 2000, Phys. Rev. D, 62, 043511
Armendariz-Picon C., 2004, J. Cosmol. Astropart. Phys., 0407, 007
Battye R. A. et al., 2012, preprint (arXiv:1209.1041)
Benitez N. et al., 2009, ApJ, 691, 241
Benitez N. et al., 2014, preprint (arXiv:1403.5237)
Blanton M. R. et al., 2017, AJ, 154, 28
Borges H. A., Wands D., 2017, preprint (arXiv:1709.08933)
Caldwell R. R., Dave R., Steinhardt P. J., 1998, Phys. Rev. Lett., 80, 1582
Chimento L. P., Jakubi A. S., Pavón D., Zimdahl W., 2003, Phys. Rev. D, 67, 083513
Costa A. A., 2014, PhD thesis, Univ. São Paulo, São Paulo http://www.teses.usp.br/teses/disponiveis/43/43134/tde-20012015-123002/
Costa A. A., Xu X.-D., Wang B., Ferreira E. G. M., Abdalla E., 2014, Phys. Rev. D, 89, 103531
Costa A. A., Olivari L. C., Abdalla E., 2015, Phys. Rev. D, 92, 103501
Costa A. A., Xu X.-D., Wang B., Abdalla E., 2017, J. Cosmol. Astropart. Phys., 1701, 028
D'Amico G., Hamill T., Kaloper N., 2016, Phys. Rev. D, 94, 103526
Dawson K. S. et al., 2016, AJ, 151, 44
DESI Collaboration, 2016, preprint (arXiv:1611.00036)
Feldman H. A., Kaiser N., Peacock J. A., 1994, ApJ, 426, 23
Frieman J. A., Hill C. T., Watkins R., 1992, Phys. Rev. D, 46, 1226
Frieman J. A., Hill C. T., Stebbins A., Waga I., 1995, Phys. Rev. Lett., 75, 2077
Gavela M., Hernández D., Honorez L. L., Mena O., Rigolin S., 2009, J. Cosmol. Astropart. Phys., 0907, 034
Giannantonio T., Porciani C., Carron J., Amara A., Pillepich A., 2012, MNRAS, 422, 2854
He J.-H., Wang B., Abdalla E., 2009, Phys. Lett. B, 671, 139
Hsu S. D. H., 2004, Phys. Lett. B, 594, 13
Kimura R., Suyama T., Yamaguchi M., Yamauchi D., Yokoyama S., 2018, PASJ, 70, L5
Landim R. G., Abdalla E., 2017, Phys. Lett. B, 764, 271
Laureijs R. et al., 2011, preprint (arXiv:1110.3193)
Lewis A., Challinor A., Lasenby A., 2000, ApJ, 538, 473
Li M., 2004, Phys. Lett. B, 603, 1
Li H., Yang W., Wu Y., Jiang Y., 2018, Phys. Dark Universe, 20, 78
LSST Science Collaboration, 2009, preprint (arXiv:0912.0201)
Maartens R., Abdalla F. B., Jarvis M., Santos M. G., 2015, Proc. Sci. Sissa, Trieste, PoS#016
Marcondes R. J., Landim R. C., Costa A. A., Wang B., Abdalla E., 2016, J. Cosmol. Astropart. Phys., 1612, 009
Marín F. A., Beutler F., Blake C., Koda J., Kazin E., Schneider D. P., 2016, MNRAS, 455, 4046
Micheletti S., Abdalla E., Wang B., 2009, Phys. Rev. D, 79, 123506
Murgia R., Gariazzo S., Fornengo N., 2016, J. Cosmol. Astropart. Phys., 1604, 014
Orsi l. A., Angulo R. E., 2018, MNRAS, 475, 2530
Orsi A., Baugh C. M., Lacey C. G., Cimatti A., Wang Y., Zamorani G., 2010, MNRAS, 405, 1006
Peebles P. J. E., Ratra B., 1988, ApJ, 325, L17
Perlmutter S. et al., 1999, ApJ, 517, 565
Rassat A. et al., 2008, preprint (arXiv:0810.0003)
Ratra B., Peebles P. J. E., 1988, Phys. Rev. D, 37, 3406
Riess A. G. et al., 1998, AJ, 116, 1009
Ross N. P. et al., 2009, ApJ, 697, 1634
Santos L., Zhao W., Ferreira E. G. M., Quintin J., 2017, Phys. Rev. D, 96, 103529
Seo H.-J., Eisenstein D. J., 2003, ApJ, 598, 720
Stojkovic D., Starkman G. D., Matsuo R., 2008, Phys. Rev. D, 77, 063006
Takada M. et al., 2014, PASJ, 66, R1
Tegmark M., 1997, Phys. Rev. Lett., 79, 3806
The Dark Energy Survey Collaboration, 2005, preprint (arxiv:astro-ph/0510346)
Väliviita J., Majerotto E., Maartens R., 2008, J. Cosmol. Astropart. Phys., 0807, 020
Wang Y. et al., 2010, MNRAS, 409, 737
Wang B., Abdalla E., Atrio-Barandela F., Pavón D., 2016, Rep. Prog. Phys., 79, 096901
Wetterich C., 1995, A&A, 301, 321
Witzemann A., Alonso D., Fonseca J., Santos M. G., 2019, MNRAS, 485, 5519
Wuensche C. A., the BINGO Collaboration, 2018, preprint (arXiv:1803.01644)
Yang W., Pan S., Di Valentino E., Nunes R. C., Vagnozzi S., Mota D. F., 2018, J. Cosmol. Astropart. Phys., 1809, 019
Zimdahl W., Pavón D., Chimento L. P., 2001, Phys. Lett. B, 521, 133

This paper has been typeset from a TEX/LATEX file prepared by the author.